

AEROSERVOELASTIC ANALYSIS OF ROTORCRAFT-PILOT INTERACTION BY COUPLED BEM-MULTIBODY SOLVERS

Pierangelo Masarati*, Giuseppe Quaranta*, Massimo Gennaretti†, and Jacopo Serafini†

*Dipartimento di Ingegneria Aerospaziale, Politecnico di Milano, Milano - Italy
{pierangelo.masarati,giuseppe.quaranta}@polimi.it

†Dipartimento di Ingegneria Meccanica e Industriale, Università Roma Tre, Roma - Italy
{m.gennaretti,serafini}@uniroma3.it

Abstract

This paper illustrates a joint effort between two research groups at Politecnico di Milano and University Roma Tre that investigates Rotorcraft-Pilot Coupling from an aeroservoelastic point of view. Coupling between helicopter dynamics and aeroservoelasticity with the passive behavior of the pilot is analyzed. The presence of the pilot in the control loop may cause the unintentional transmission of the vibratory motion of the rotorcraft through the control inceptors. This work addresses in detail the interaction of the pilot with the collective lever, which may cause the 'vertical bounce' of the aircraft. The parameters that mainly affect the phenomenon in hover and forward flight are analyzed to infer design guidelines.

INTRODUCTION

Aircraft pilots should be considered, from the dynamics point of view, as the element that creates a feedback loop, closing the path between the aircraft motion, sensed by the pilots' body, and its control, realized through the cockpit inceptors grasped by the pilots' hands. As well known in control theory, such feedback, if associated with the appropriate gain or phase delay, can result in a degradation of performances and handling qualities. In the worst cases, the pilot can destabilize the system, as noted by McRuer [1]. The couplings are usually classified in two main categories: those related to a voluntary intervention, called Pilot-Induced Oscillations (PIO), and those related to an involuntary intervention, called Pilot-Assisted Oscillations (PAO).

The problem has been investigated in detail with respect to fixed-wing aircraft, as testified by the literature (see [1] for references). Since the 1970s, key issues of Aircraft-Pilot Coupling (APC) have been identified, and effective active pilot models have been proposed and developed (see e.g. [2]). However, its implications on rotorcraft dynamics and aeroelasticity are not as well understood. Again, issues related to PIOs and flight mechanics in general are relatively well understood (see e.g. [3]). Much less literature related to PAOs and

aeroelasticity is available.

The passive biomechanics of rotorcraft pilots has been studied, for example, by Mayo [4]. It has been taken into account by Bell Helicopter during the development of the V-22 tiltrotor aircraft [5], and incorporated in the design of the BA609 [6]. Reports of Rotorcraft-Pilot Coupling (RPC) occurred to US Navy helicopters during development and initial deployment and operation have been recently presented by Walden [7].

During an exploratory activity performed by GARTEUR HC AG-16, a classification in terms of frequency range has been proposed [8]. PIOs are recognized as basically related to flight dynamics, in the range up to 1Hz, while PAOs typically occur at frequencies between 2 and 8Hz, and are related to aeroelastic phenomena. This distinction is relatively straightforward for fixed-wing aircraft. However, rotary-wing aircraft show significant overlapping, since a broad band of frequencies impacts flight dynamics while being close to pilot limbs' intrinsic frequencies. Figure 1 illustrates typical rotary-wing frequency bandwidth.

MODELING AND ANALYSIS APPROACH

The approach followed in this activity consists in analyzing the rotorcraft aeromechanics aspects that impact their coupling with the pilot's passive

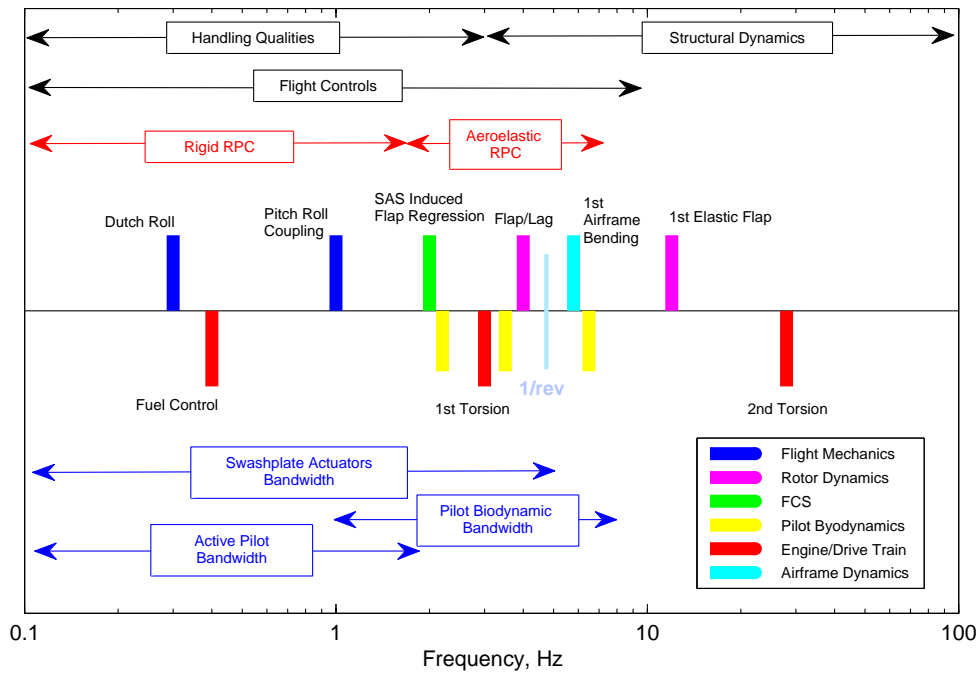


Figure 1: Typical rotorcraft frequency bandwidth.

biomechanics. Aeroservoelastic models of rotorcraft are used to describe relevant aspects including: main and tail rotor aeromechanics and aeroelasticity, airframe dynamics, control systems servodynamics.

Pilot Biomechanics

The pilot may alter the dynamics of a rotorcraft in different manners. When the pilot intentionally enters a command in order to perform some task the intervention is voluntary. Sometimes the intervention can be introduced with a significant delay compared with the characteristic time of the movement that must be controlled, eventually increased by the presence of the FCS. In other situations the input can be altered by erroneous perceptions, This type of intervention is nonetheless band-limited by the capabilities of human limbs; as such, any phase shifting it may cause is likely to affect the very low-frequency modes that characterize flight mechanics.

The pilot may also input commands unintentionally, as a consequence of excitations coming from the cockpit environment. For example, the vibration of the seat, or of other parts of the cockpit, may induce unintentional motion of the control in-

ceptors, filtered by the passive dynamics of the pilot's limbs.

The phenomenon known as 'vertical bounce', or 'collective bounce', is characteristic of helicopters, consisting in a vertical oscillation caused by pulsating thrust induced by an oscillation unintentionally introduced in the collective control by the pilot. The motion of the collective control essentially results in a direct change of blade pitch, and thus in a very quick change in thrust. Even recently, the National Transportation Safety Board (NTSB) reported accidents occurred after encountering collective bounce (NTSB reports SEA08LA043 and ANC08LA083, respectively related to accidents occurred in December 2007 and June 2008). In both cases a UH-1B was involved; the probable cause was related to failure of the pilot in controlling the vertical bounce. In one case this was accompanied by insufficient collective control friction; in the other, to poor maintenance, resulting in loose and worn control system and rotor bearings. The NTSB reports indicate collective bounce as a pilot-induced vertical oscillation that may be encountered in any flight condition by a rapid buildup of vertical bounce at approximately three cycles per second. The resulting severe oscillations may make the effective control of the aircraft difficult

Table 1: Coefficients of transfer functions from [4].

	Mesomorphic	Ectomorphic
a_0	555.4	452.3
a_1	13.31	13.70
b_0	555.4	452.3
b_1	4.02	5.19

to maintain. A different although related type of collective bounce is associated to carrying slung loads with a deformable cable.

Initially, the passive biomechanics of the pilot has been considered for specific controls, e.g. collective when undergoing vertical bounce, using transfer functions available from the literature [4, 9, 10]. Mayo [4] identified the transfer function between the vertical acceleration of a helicopter's seat and the tangential acceleration of the collective stick close to the handle, using an instrumented cockpit mock-up subjected to harmonic excitation. Second-order transfer functions of the form

$$H = \frac{b_1 s + b_0}{s^2 + a_1 s + a_0} \quad (1)$$

have been identified by testing a set of volunteers. They have been grouped in the so-called 'mesomorphic' (larger size) and 'ectomorphic' (smaller size) models; the corresponding coefficients are reported in Table 1 and the transfer functions are illustrated in Fig. 2. Both functions present two complex conjugate poles. The mesomorphic poles are at 3.6 Hz, with slightly less than 30% damping, while the ectomorphic ones are at 3.2 Hz, with a slightly higher damping. According to [4], the gain of these functions must be parametrized with respect to the reference collective setting. How these functions need to be modified to fit the requirements of time marching analysis is discussed in a later section.

Similar transfer functions have been subsequently identified from results obtained in specific test campaigns performed in cooperation with the University of Liverpool using the 'Bibby' flight simulation facility [10, 11, 12]. They have been applied to the aeroservoelastic analysis of rotorcraft [13]. Those functions actually represent the relative rotation of the collective inceptor as a function of the vertical acceleration of the seat. Different subjects and different reference collective settings were considered, highlighting how the reference collective not only scales the gain of the transfer function, but also changes the frequency and the damping. Figure 3 illustrates the function related

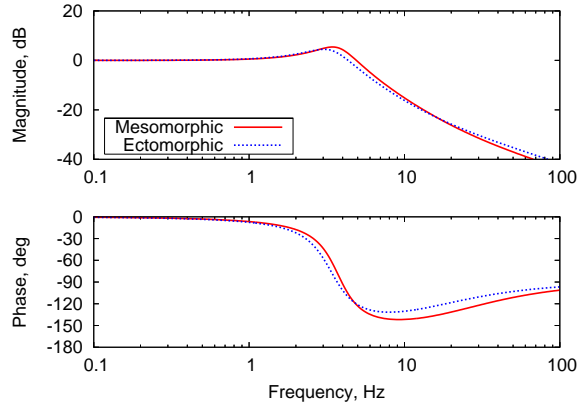


Figure 2: Pilot transfer functions [4].

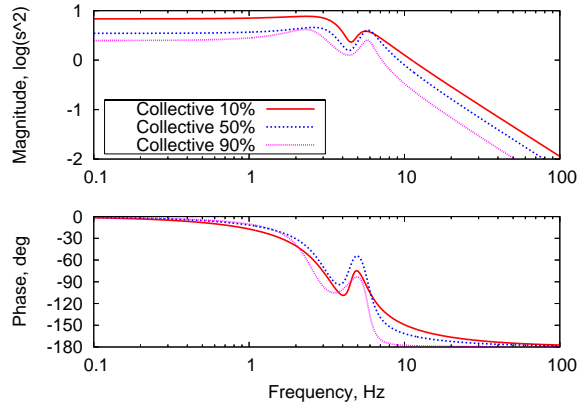


Figure 3: Pilot transfer functions [13].

to one pilot for different reference collective settings. These functions are characterized by two pairs of poles and two zeros. The lower frequency poles are very close to the high frequency ones of Mayo, between 3 and 3.6Hz, while the others are between 5 and 6.5Hz, depending on the subject and the reference collective. The presence of this second mode is indirectly confirmed by in-flight measurements of pilot's limb vibrations conducted during collective dwell tests of the BA-609 with different levels of control friction [14]. As pointed out in [10], in some configurations the higher frequency pole might approach instability earlier than the lower frequency one. The experimental evidence of the fundamental passive pilot frequency related to the collective control explains the "three cycles per second" oscillation the UH-1B manual indicates as characteristic of that helicopter's vertical bounce. Helicopters of the same class and of similar classes may present similar characteristics. The influence of unsteady aerodynamics and airframe dynamics modeling on RPC proneness was

investigated as well [13, 15].

Critical aspects of rotorcraft aeroservoelasticity coupled to passive pilot biomechanics have been identified in:

- determining the most appropriate aeroelastic modeling detail level that allows to capture the essence of the phenomenon within efficient simulations;
- determining pilot models suitable for identifying the proneness to RPC of specific rotorcraft configurations and flight conditions.

The phase of the work presented in this paper addresses the integration of aerodynamics and structural dynamics modeling capabilities independently developed by the partners, to exploit the respective points of strength.

Structural Dynamics

The structural dynamics of the helicopter is modeled using the free general-purpose multibody solver MBDyn (<http://www.mbdyn.org/>), developed by the Aeroservoelasticity and Structural Dynamics research group of the ‘Dipartimento di Ingegneria Aerospaziale’, Politecnico di Milano. The approach is quite general: the multibody solver can directly address many aspects of the problem, including aeroelasticity itself, although built-in aerodynamics is limited to Blade Element/Momentum Theory. For this reason, in this work aerodynamics is delegated to an external solver, discussed in the next section.

The structural model consists of the main rotor and the airframe. The rotor is modeled using the multibody approach: kinematically exact constraints, enforced by means of Lagrange multipliers, describe the relative motion between rigid bodies, while structural dynamics is dealt with by a Finite Element (FE)-like approach using nonlinear, geometrically exact beam elements based on an original Finite Volume (FV) formulation [16], and by lumped masses.

The airframe is modeled using the Component Mode Synthesis (CMS) approach. It is connected to the rotor by a revolte joint that enforces the relative rotation. The interface between the CMS model and the multibody domain occurs at selected points, including the main (and tail, when needed) rotor attachment, and the pilot’s and co-pilot’s seats. The CMS model consists of selected Normal Vibration Mode (NVM) shapes, whose frequency is within the range of interest, and with a non-negligible participation of the rotor attachment

and crew seat motion. The NVM have been computed with the rotor mass lumped at the connection point. The rotor mass has been subsequently removed from the modal mass matrix, since it is already contributed by the multibody model.

Although a complete model of the free-flying helicopter, including the tail rotor, has been developed, for the purpose of this investigation the overall rigid-body motion of the helicopter is selectively constrained to enforce the desired flight condition. Only the rigid-body degrees of freedom deemed important for each specific analysis are allowed.

Aerodynamics

The aerodynamics governing the forces acting on helicopters is dominated by the unsteady behavior of the main rotor and its inflow on the tail rotor and the other aerodynamic surfaces. The accurate analysis of problems involving interaction between vortices and bodies requires the application of suited three-dimensional, unsteady aerodynamic solvers. The boundary integral formulation for potential flows introduced in [17], developed by the Aeroelasticity research group of the ‘Dipartimento di Ingegneria Meccanica e Industriale’, Università Roma Tre, is applied in this work.

It represents an enhancement of the formulation proposed in [18]. It overcomes numerical solution instabilities caused by the impingement of the wake on body surfaces, It introduces the decomposition of the potential field into an incident field, φ_I , and a scattered field, φ_S . The scattered potential is generated by sources and doublets over the body surfaces, and by doublets over portions of the body wakes very close to the trailing edges they emanated from (near wake, S_W^N). The incident potential is generated by doublets over the complementary wake regions that compose the far wakes, S_W^F . These wake portions may impinge on other surfaces. The scattered potential is discontinuous across S_W^N , whereas the incident potential is discontinuous across S_W^F . Hence, as demonstrated in [17], for $\varphi = \varphi_I + \varphi_S$ the scattered potential is obtained by

$$\begin{aligned} \varphi_S(\mathbf{x}, t) = & \int_{S_B} \left[G(\chi - \chi_I) - \varphi_S \frac{\partial G}{\partial n} \right] dS(\mathbf{y}) \\ & - \int_{S_W^N} \Delta\varphi_S \frac{\partial G}{\partial n} dS(\mathbf{y}), \end{aligned} \quad (2)$$

where G is the unit source solution and $\Delta\varphi_S$ is the potential jump across the wake surface [17]. In addition, $\chi = \mathbf{v} \cdot \mathbf{n}$ accounts for the impenetrability boundary condition (\mathbf{v} denotes the body velocity

due to rigid and elastic body motion; \mathbf{n} is the surface unit outward normal vector), while $\chi_I = \mathbf{u}_I \cdot \mathbf{n}$, with the velocity induced by the far wake, $\mathbf{u}_I = \nabla\phi_I$, given by

$$\mathbf{u}_I(\mathbf{x}, t) = -\nabla \int_{S_W^f} \Delta\phi_S \frac{\partial G}{\partial n} dS(\mathbf{y}) \quad (3)$$

The incident potential affects the scattered potential by the induced-velocity term, χ_I ; in turn, the scattered potential affects the incident potential by its trailing-edge discontinuity that is convected along the wake and yields the intensity of the doublet distribution over the far wake.

Obtaining the zero-th order discrete form of Eq. (3) by using N panels over the far wakes, and recalling the vortex-doublet equivalence, the incident velocity field may be evaluated using

$$\mathbf{u}_I(\mathbf{x}, t) \approx -\sum_{n=1}^N \Delta\phi_S(\mathbf{y}_{W_n}^{TE}, t - \theta_n) \int_{C_n} \nabla_{\mathbf{x}} G \times d\mathbf{y}$$

where C_n denotes the contour line of the n -th far wake panel, $\mathbf{y}_{W_n}^{TE}$ is the trailing edge position where the wake material point currently in \mathbf{y}_{W_n} emanated at time $t - \theta_n$, and $\nabla_{\mathbf{x}}$ denotes the gradient with respect to \mathbf{x} . This equation represents the velocity field given by the Biot-Savart law applied to the vortices having the shape of the far wake panel contours and intensity $\Delta\phi_S(\mathbf{y}_{W_n}^{TE}, t - \theta_n)$. A finite-thickness core is introduced in these vortices where a regular distribution of the induced velocity is assured, along with a stable and regular solution even in body-vortex impact conditions [17] (this may only affect the far wake).

Once the potential field is known, the Bernoulli theorem yields the pressure distribution. The corresponding aerodynamic loads are obtained by integration over the body surface.

Fluid-Structure Interface

The coupling of the aerodynamic BEM solver to the free general-purpose multibody solver MB-Dyn represents a key aspect of this study. The two solvers are run as separate processes, and communicate using standard UNIX sockets. The multibody solver sends information about the kinematics of the structure to the aerodynamic solver, and receives the aerodynamic loads in response. The two domains are mapped using a linear projection that extracts generalized information from the beam-based FEM modeling of the rotor. The generalized loads provided by the BEM solver are projected back on the FEM nodes of the multibody model by the conjugated projector. This

guarantees that both models experience the same amount of work done by the interface forces for the interface displacement [19].

Consider the arbitrary absolute motion of node i , described by its orientation \mathbf{R}_i and location \mathbf{x}_i . When referred to the motion of node r , it is

$$\tilde{\mathbf{R}}_i = \mathbf{R}_r^T \mathbf{R}_i \quad (4a)$$

$$\tilde{\mathbf{x}}_i = \mathbf{R}_r^T (\mathbf{x}_i - \mathbf{x}_r). \quad (4b)$$

The differentiation of arbitrary rotations is defined in terms of the derivative of the orientation matrix. For example, the angular velocity ω_i is defined as $\omega = \text{ax}(\dot{\mathbf{R}}\mathbf{R}^T)$, where $\text{ax}(\cdot)$ is the inverse of the cross-product operator $(\cdot) \times$. The linear and angular velocity of node i are

$$\tilde{\omega}_i = \mathbf{R}_r^T (\omega_i - \omega_r) \quad (5a)$$

$$\dot{\tilde{\mathbf{x}}}_i = \mathbf{R}_r^T (\dot{\mathbf{x}}_i - \dot{\mathbf{x}}_r) + \tilde{\mathbf{x}}_i \times \mathbf{R}_r^T \omega_r. \quad (5b)$$

When the relative motion is small enough to be approximated linearly by a set of shape functions $\mathbf{H}_x, \mathbf{H}_R$ weighted by the multipliers \mathbf{q} , it results in

$$\tilde{\mathbf{R}}_i \cong \tilde{\mathbf{R}}_i(\mathbf{H}_R \mathbf{q}) \quad (6a)$$

$$\tilde{\mathbf{x}}_i \cong \tilde{\mathbf{x}}_{0i} + \mathbf{H}_x \mathbf{q}. \quad (6b)$$

As soon as $\tilde{\theta}_i \cong \mathbf{H}_R \mathbf{q}$ is small enough, the first-order approximation

$$\tilde{\mathbf{R}}_i \cong \mathbf{I} + (\mathbf{H}_R \mathbf{q}) \times \quad (7)$$

can be used.

After defining $\tilde{\theta}_\delta$ and $\delta\tilde{\mathbf{x}}$ as the collection of the virtual rotations and displacements of all nodes, and $\delta\mathbf{q}$ as the virtual perturbations of the modal variables, the mapping

$$\begin{bmatrix} \mathbf{H}_x \\ \mathbf{H}_R \end{bmatrix} \delta\mathbf{q} = \begin{Bmatrix} \delta\tilde{\mathbf{x}} \\ \tilde{\theta}_\delta \end{Bmatrix} \quad (8)$$

can be inverted, using the Moore-Penrose Generalized Inverse (MPGI), or pseudo-inverse, to yield the projection matrix \mathbf{H}^+ that projects the virtual relative motion of the nodes onto the space of the modal variables \mathbf{q} , namely

$$\mathbf{q} = \mathbf{H}^+ \begin{Bmatrix} \tilde{\mathbf{x}} - \tilde{\mathbf{x}}_0 \\ \tilde{\theta} \end{Bmatrix}. \quad (9)$$

The same transformation allows to project the velocities,

$$\dot{\mathbf{q}} = \mathbf{H}^+ \begin{Bmatrix} \dot{\tilde{\mathbf{x}}} \\ \dot{\tilde{\omega}} \end{Bmatrix}. \quad (10)$$

According to the Virtual Work Principle (VWP), the virtual work of nodal forces and moments, $\tilde{\mathbf{f}}$ and $\tilde{\mathbf{m}}$, is equal to that of the generalized forces \mathbf{p} ,

$$\tilde{\boldsymbol{\theta}}_8^T \tilde{\mathbf{m}} + \delta \tilde{\mathbf{x}}^T \tilde{\mathbf{f}} = \delta \mathbf{q}^T \mathbf{p}. \quad (11)$$

The virtual perturbation of the mapping of Eq. (9) yields the nodal forces

$$\begin{Bmatrix} \tilde{\mathbf{f}} \\ \tilde{\mathbf{m}} \end{Bmatrix} = (\mathbf{H}^+)^T \mathbf{p}, \quad (12)$$

whose virtual work is equivalent to that of the corresponding generalized forces. In the absolute frame, they result in

$$\mathbf{f}_i = \mathbf{R}_r \tilde{\mathbf{f}}_i \quad i \neq r \quad (13a)$$

$$\mathbf{f}_i = -\mathbf{R}_r \sum_j \tilde{\mathbf{f}}_j \quad i = r \quad (13b)$$

$$\mathbf{m}_i = \mathbf{R}_r \tilde{\mathbf{m}}_i \quad i \neq r \quad (13c)$$

$$\mathbf{m}_i = -\mathbf{R}_r \sum_j (\tilde{\mathbf{f}}_j + \tilde{\mathbf{x}}_j \times \tilde{\mathbf{f}}_j) \quad i = r. \quad (13d)$$

The contributions to force and moment in node r need to be added (actually, subtracted according to Eqs. (13b) and (13d)) to the corresponding rigid-body rotor force and moment computed by the BEM solver.

The BEM solver models the deformation of the blade as the linear combination of lag, flap and torsion modes, including rigid modes (i.e. articulated rotor lag and flap, and rigid pitch) if needed. The shape functions for bending and torsion are

$$Y_k = \cosh(\beta_k \xi) - \cos(\beta_k \xi) - \alpha_k (\sinh(\beta_k \xi) - \sin(\beta_k \xi)) \quad (14a)$$

$$\Theta_k = \sqrt{2} \sin((k-1/2)\pi \xi), \quad (14b)$$

where ξ is a non-dimensional abscissa ranging from 0 at the beginning of the deformable portion of the blade to 1 at the tip, while coefficients α_k are

$$\alpha_k = \frac{\cosh(\beta_k) + \cos(\beta_k)}{\sinh(\beta_k) + \sin(\beta_k)} \quad (15)$$

and β_k correspond to the clamp-free boundary conditions for a uniform beam, asymptotically yielding $\lim_{k \rightarrow \infty} \beta_k = (k-1/2)/\pi$. These functions are mapped on the relative displacements with respect to a reference undeformed blade configuration of the multibody nodes of the main rotor.

The coupling procedure, from the point of view of the multibody solver, is:

1. transform the configuration of participating structural nodes in the reference frame of node r according to Eqs. (4) and (5);

2. compute modal variables and their derivatives according to the mapping of Eqs. (9) and (10);
3. pass the mapped motion and the motion of node r to the BEM solver;
4. receive the generalized forces and the rigid-body forces and moments from the BEM solver;
5. transform generalized forces in nodal forces and moments according to Eq. (12);
6. transform nodal forces from the reference frame of node r into the absolute reference frame according to Eqs. (13).

A tight coupling has been implemented. The two solvers communicate at the iteration level, thus converging cooperatively within each time step. In most analysis, however, the wake geometry can be considered frozen within the time step. In those cases, the coupling, although formally tight, actually consists in a single exchange. After it, the multibody solver iterates as required to converge with fixed aerodynamic loads.

This approach allows to exploit the points of strength of the BEM and of the multibody solver in the analysis of this intrinsically multidisciplinary problem. In fact, as reported in earlier analyses [13], the appearance of adverse couplings is related to simultaneously considering: a) pilot's feedthrough, b) rigid-body motion of the rotorcraft, c) compliance of the blades and d) of the airframe, all coupled by the aerodynamics of the rotor.

Coupling with the Pilot

The pilot models are coupled with the system within the multibody solver. General-purpose elements (GENELs) allow to model arbitrary system dynamics. In this case, the pilot is modeled as a State Space (SS) representation of a Multi-Input Multi-Output (MIMO) system. It receives in input the absolute accelerations of the seat, and outputs the motion of the control inceptors, namely the collective bar and the cyclic stick. In this work, only the collective control is considered.

The transfer functions proposed by Mayo [4] describe the absolute acceleration of the collective handle with respect to the absolute acceleration of the seat. They need to be transformed into the (relative) rotation of the collective bar as a function of the vertical acceleration of the seat. The relative acceleration is described by $H_{\text{rel}}(s) = H_{\text{abs}}(s) - 1$.

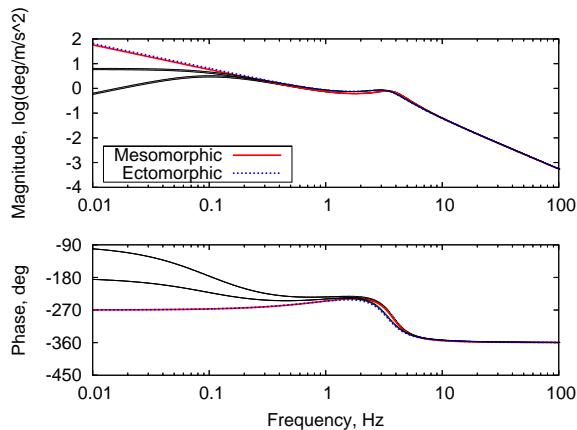


Figure 4: Pilot transfer functions of Figure 2, modified to yield the relative rotation.

The relative rotation of the bar is obtained by dividing the relative acceleration by the length of the collective bar, L , and by integrating twice,

$$\Delta\theta(s) = \frac{1}{s^2} \frac{1}{L} (H_{\text{abs}}(s) - 1) a(s). \quad (16)$$

When this transformation is applied to Eqs. (1), the transfer functions of Fig. 4 result. The presence of two integrators $1/s^2$ in Eq. (16) yield a drifting behavior when $s \rightarrow 0$. This is not physical, as it would imply, for example, that the collective reduces indefinitely because of gravity. What this experimental transfer function is missing is the fact that the pilot's active behavior will compensate any low-frequency change of collective inceptor position as soon as it is adequately detected.

In order to take this into account, the functions are high-pass filtered, by simply turning the integrator poles $1/s^2$ into real poles close to zero, namely

$$\Delta\theta(s) = \frac{1}{(s - \alpha_1)(s - \alpha_2)} \frac{1}{L} (H_{\text{abs}}(s) - 1) a(s). \quad (17)$$

The dashed lines in Fig. 4 illustrate this correction. They correspond to turning either one or both the integrators into one or two poles at 0.1Hz. The 'active' pilot behavior, in the simulation, is delegated to a simple PD regulator with very low gains, in order to minimize its interaction with the dynamics of the system in the frequency range of interest, while loosely flying the helicopter in the desired flight condition. This pilot model is roughly analogous to Hess' Structural Pilot Model (SPM) [20], with emphasis on the biomechanical behavior.

The outputs are transformed into swashplate commands after additional filtering, intended to

represent the dynamics of the actuation system. For example, the dynamics of the hydraulic actuators that command the swashplate motion are typically expressed using first- or second-order transfer functions, e.g. $y = 1/(1 + \tau s)u$ or $y = 1/(1 + 2\zeta s/\omega_0 + s^2/\omega_0^2)u$, where u is the actuator elongation commanded by the pilot, while y is the resulting elongation.

In principle, within the multibody approach the impedance of the actuators can be considered, and nonlinear effects like friction, saturation, freeplay, backlash can be added. These effects, for example, may characterize Cat. II PIO [1]. However, they are beyond the scope of this work, as they typically impact RPC related to 'intentional' inputs given by the pilot.

NUMERICAL RESULTS

Model Description

The model consists of a light helicopter, loosely inspired by the Bo105. The same rotorcraft was used in [8]. One of the reasons is that a considerable amount of information on the Bo105 has been publicly available for a long time (e.g. [21]).

The structural model consists in up to 4 airframe modes, with 2% structural damping. The first one, at about 6Hz, is of most relevance for the vertical bounce of the rotorcraft, since it consists in the bending of the airframe in the $x-z$ plane. Its mode shape presents a non-negligible vertical motion of the main rotor attachment node and of the pilot and co-pilot nodes. The cockpit nodes move in phase opposition with respect to the main rotor attachment.

Each blade of the main rotor is modeled using 5 three-node beam elements, resulting in 11 structural nodes per blade. This discretization guarantees a very accurate description of the dynamics of the lower rotating blade modes and, at the same time, results in a fairly efficient model from a computational cost viewpoint.

The aerodynamic kinematics is modeled using 3 lag and 3 flap bending modes, and the rigid pitch and 2 torsion modes per blade. Various aerodynamic discretization levels (chordwise and spanwise blade discretization, and wake history) have been considered, to find a good trade-off between accuracy and computational time. As a reference, a quasi-steady Blade Element/Momentum Theory (BE/MT) aerodynamic model has been considered as well. The swashplate actuators are modeled using first-order transfer functions with $\tau = 0.04s$.

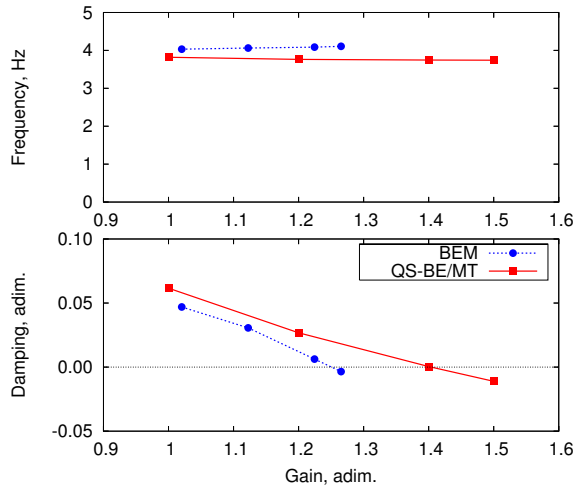


Figure 5: Frequency/damping of pilot mode vs. gain in hover (pilot model from [4]).

As one would expect, the BEM approach requires more computational effort than the simpler BE/MT, depending on the aerodynamic discretization of the blades and of the wake. In some cases, during the co-simulation, more than 90% of the computational time was consumed by the aerodynamic solver.

Vertical Bounce: Hover

With respect to vertical bounce, the pilot mode (about 3.5Hz when uncoupled) appears to couple with both the first airframe mode (slightly less than 6Hz) and with the collective flap bending mode (about 7Hz). The excitation comes from the vertical acceleration of the pilot's seat, composed of rigid body motion and airframe deformation. The corresponding collective inceptor motion (a relative rotation) is transformed by the swashplate into a change of blade pitch. The ratio between the collective lever rotation and the blade pitch is a design parameter. The inceptor must be able to cover the whole range of blade pitch required to control the helicopter within a comfortable range of pilot's arm positions.

A fictitious 'pilot gain' is introduced between the transfer function of the pilot and that of the swashplate actuators. It is worth stressing that this parameter is by no means related to any 'aggressiveness' in the pilot's behavior. It is rather related to determining what choice of design parameters can endanger stability when the pilot is in the loop. This gain can include many aspects of the problem: a change in modal amplitude of the seat's motion, a

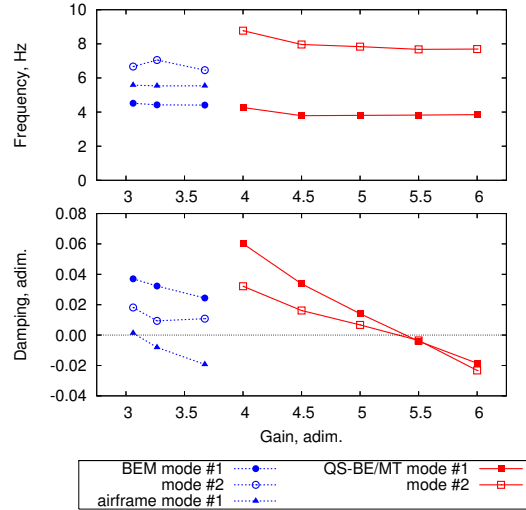


Figure 7: Frequency/damping of pilot mode vs. gain in hover (pilot model from [11]).

modification of the rate between the collective inceptor rotation and the blade pitch, and so on.

Figure 5 shows how the pilot's gain may drive the mode associated to the pilot's biodynamics unstable. The mesomorphic pilot model proposed in [4] is used, modified according to Eq. (17) with $\alpha_1 = 0$ and $\alpha_2 = 0.1 \cdot 2\pi$. It also shows that the BEM aerodynamic model predicts the instability at a slightly lower gain level. This is consistent with the results anticipated in [22]. The equivalent frequency and damping ratio has been identified from the transient response to an excitation introduced with the collective, using the technique proposed in [23], based on Proper Orthogonal Decomposition (POD). Figure 6 illustrates a detail of the motion of the main rotor blades at instability.

Figure 7 shows similar results obtained using the pilot model identified in [11], characterized by two modes. When using BE/MT, the two pilot modes become unstable almost simultaneously, at a gain level higher than required in the previous case. When using BEM, the first airframe mode becomes unstable first, at a lower gain level.

Reasonable values had to be chosen for all the unknown parameters involved in this problem. This justifies the significant differences in behavior of the different pilot models. The appearance of an instability at gain levels slightly above unit by no means implies that the Bo105, or rotorcraft of the same class, are specifically prone to this type of PAO. The main indication one can expect from this analysis is that the coupling mechanism investigated in this study may qualitatively and, to some

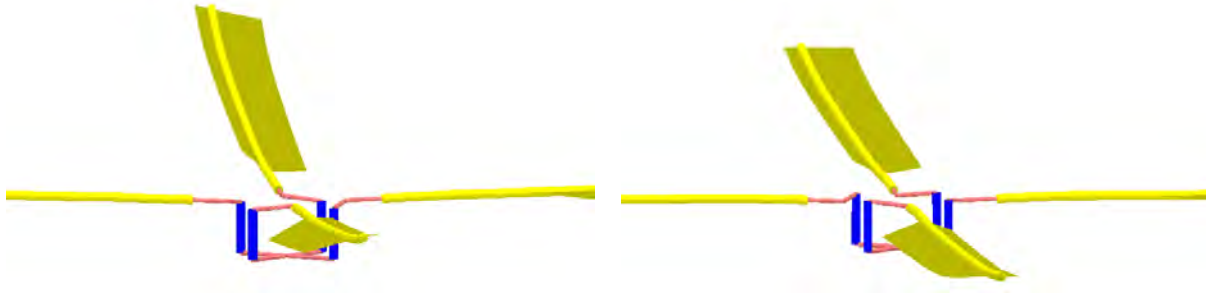


Figure 6: Collective flap mode at instability in hover (pilot model from [4]).

extent, quantitatively explain a well known type of instability.

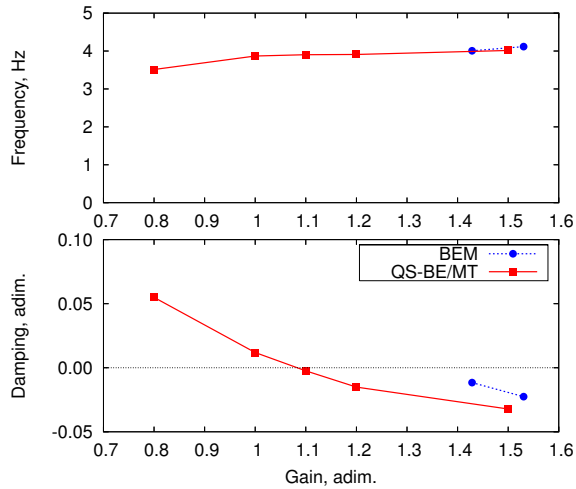


Figure 8: Frequency/damping of pilot mode vs. gain in forward flight, $\mu = 0.1$ (pilot model from [4]).

Vertical Bounce: Forward Flight

The rotorcraft has been trimmed at an advance ratio $\mu = 0.1$, and the same analysis of the hover case has been performed. Figure 8 illustrates the dependence of the pilot mode's frequency and damping on the pilot's gain. Figure 9 illustrates the results related to the pilot model identified in [11]. The first airframe mode is also shown, because it becomes unstable first. As soon as the pilot's second mode couples with the first airframe mode, it becomes unsteady as well, while the damping of the pilot's first mode appears to be only marginally affected by the gain. This preliminary result seems to indicate that focusing on the pilot's first mode may hide other instability mechanisms.

Only limited results in forward flight have been obtained so far with the coupled aeroelastic solver

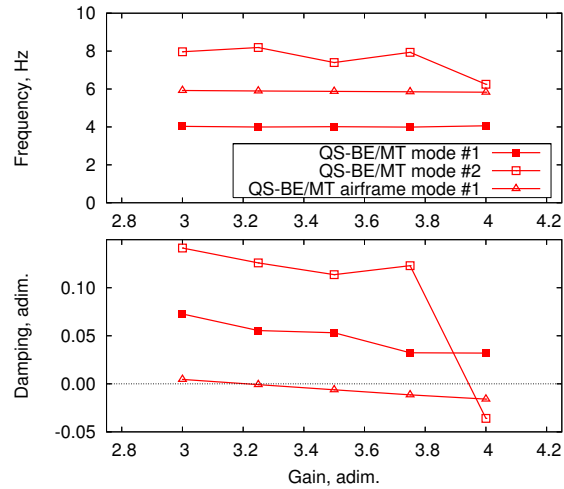


Figure 9: Frequency/damping of pilot mode vs. gain in forward flight, $\mu = 0.1$ (pilot model from [11]).

because of convergence issues that have not been completely solved yet. Further investigation is needed in order to confirm these results.

CONCLUDING REMARKS

The coupling of a general-purpose multibody dynamics solver with a boundary element method aerodynamic solver has been developed and applied to the analysis of rotorcraft-pilot interaction, focusing on vertical bounce in hover and in forward flight. The aim is to improve the level of refinement in the analysis of aeroelastic rotorcraft-pilot interaction. The suitability of the proposed simulation framework is illustrated by the capability to predict the interactional phenomenon for a realistic aeroservoelastic model of a helicopter. The comparison of the results with those obtained using simpler aerodynamic models is encouraging. Future development will address the complete analysis of the flight envelope of realistic helicopter mod-

els, including stationary maneuvers, and the analysis of rotorcraft-pilot interaction through the cyclic control.

ACKNOWLEDGMENTS

The authors acknowledge partial support from the Italian Ministry of University and Research (MIUR) under PRIN 2007-8TJFZE.

REFERENCES

- [1] D. T. McRuer. *Aviation Safety and Pilot Control: Understanding and Preventing Unfavourable Pilot-Vehicle Interactions*. Washington DC: National Research Council, National Academy Press, 1997.
- [2] D. T. McRuer and E. S. Krendel. Mathematical models of human pilot behavior. Paper No. 146, Systems Technology, Inc., 13766 S. Hawthorne Boulevard Hawthorne, California 90250-7083, January 1974. AGARD AG 188.
- [3] G. D. Padfield. *Helicopter Flight Dynamics: The Theory and Application of Flying Qualities and Simulation Modeling*. AIAA Education Series, 1996.
- [4] J. R. Mayo. The involuntary participation of a human pilot in a helicopter collective control loop. In *15th ERF*, pages 81.1–12, Amsterdam, The Netherlands, 12–15 September 1989.
- [5] T. Parham Jr. and D. Popelka. V–22 pilot-in-the-loop aeroelastic stability analysis. In *47th Annual Forum of the American Helicopter Society*, Phoenix, Arizona (USA), May 6–8 1991.
- [6] T. Parham Jr. and L. M. Corso. Aeroelastic and aeroservoelastic stability of the BA 609. In *25th ERF*, Rome, Italy, September 14–16 1999.
- [7] R. B. Walden. A retrospective survey of pilot-structural coupling instabilities in naval rotorcraft. In *63rd Annual Forum of the American Helicopter Society*, Virginia Beach, VA, May 1–3 2007.
- [8] O. Dieterich, J. Götz, B. DangVu, H. Haverdings, P. Masarati, M. Pavel, M. Jump, and M. Gennaretti. Adverse rotorcraft-pilot coupling: Recent research activities in europe. In *34th ERF*, Liverpool, UK, September 16–19 2008.
- [9] P. Masarati, G. Quaranta, J. Serafini, and M. Gennaretti. Numerical investigation of aeroservoelastic rotorcraft-pilot coupling. In *XIX Congresso Nazionale AIDAA*, Forlì, Italy, September 17–21 2007.
- [10] M. Mataboni, A. Fumagalli, M. Jump, P. Masarati, and G. Quaranta. Biomechanical pilot properties identification by inverse kinematics/inverse dynamics multibody analysis. In *ICAS 2008*, Anchorage, Alaska, USA, September 14–19 2008.
- [11] M. Jump, S. Hodge, B. DangVu, P. Masarati, G. Quaranta, M. Mataboni, M. Pavel, and O. Dieterich. Adverse rotorcraft-pilot coupling: The construction of the test campaigns at the university of liverpool. In *34th ERF*, Liverpool, UK, September 16–19 2008.
- [12] M. Mataboni, G. Quaranta, P. Masarati, and M. Jump. Experimental identification of rotorcraft pilots' biodynamic response for investigation of PAO events. In *35th ERF*, pages 1–12, Hamburg, Germany, September 22–25 2009.
- [13] M. Gennaretti, J. Serafini, P. Masarati, G. Quaranta, and O. Dieterich. Aeroelastic and biodynamic modeling for stability analysis of rotorcraft-pilot coupling phenomena. In *34th ERF*, Liverpool, UK, September 16–19 2008.
- [14] P. Masarati, G. Quaranta, W. Basso, R. Bianco-Mengotti, and C. Monteggia. Biodynamic tests for pilots' characterization on the BA–609 fly-by-wire tiltrotor. In *XX AIDAA Congress*, Milano, Italy, June 29–July 3 2009.
- [15] J. Serafini, M. Gennaretti, and G. Coppotelli. Influence of fuselage dynamics properties on rotorcraft-pilot coupling phenomena. In *XX AIDAA Congress*, Milano, Italy, June 29–July 3 2009.
- [16] G. L. Ghiringhelli, P. Masarati, and P. Mantegazza. A multi-body implementation of finite volume beams. *AIAA Journal*, 38(1):131–138, January 2000. doi:10.2514/2.933.
- [17] M. Gennaretti and G. Bernardini. Novel boundary integral formulation for blade-vortex interaction aerodynamics of helicopter rotors. *AIAA Journal*, 45(6):1169–1176, 2007. doi:10.2514/1.18383.
- [18] L. Morino. A general theory of compressible potential aerodynamics. CR 2464, NASA, 1974.
- [19] G. Quaranta, P. Masarati, and P. Mantegazza. A conservative mesh-free approach for fluid structure interface problems. In *Coupled Problems 2005*, Santorini, Greece, May 24–27 2005.
- [20] R. A. Hess. Theory for aircraft handling qualities based upon a structural pilot model. *Journal of Guidance, Control and Dynamics*, 12(6):792–797, 1989. doi:10.2514/3.20483.
- [21] J. Stoppel and M. Degener. Investigations of helicopter structural dynamics and a comparison with ground vibration tests. *J. Am. Helicopter Society*, 27(2):34–42, April 1982. doi:10.4050/JAHS.27.34.
- [22] J. Serafini, L. Greco, and M. Gennaretti. Prediction of rotorcraft-pilot coupling phenomena through reduced-order aerodynamic model. In *IFASD 2009*, Seattle, Washington, June 22–24 2009.
- [23] G. Quaranta, P. Masarati, and P. Mantegazza. Assessing the local stability of periodic motions for large multibody nonlinear systems using POD. *Journal of Sound and Vibration*, 271(3–5):1015–1038, 2004. doi:10.1016/j.jsv.2003.03.004.